

# Preliminary catalogue of natural and anthropogenic VLF radio spectral patterns

Michal HOFFMAN<sup>1,2</sup> 

<sup>1</sup> Comenius University in Bratislava, Faculty of Science, Department of Engineering Geology, Hydrogeology and Applied Geophysics,  
Mlynská dolina, Ilkovičova 6, SK-842 15 Bratislava, Slovak Republic;  
e-mail: hoffman2@uniba.sk

<sup>2</sup> Earth Science Institute, Slovak Academy of Sciences,  
P.O. Box 106, Dúbravská cesta 9, SK-840 05, Bratislava, Slovak Republic

**Abstract:** Radio signals originating from natural and artificial (anthropogenic) sources were captured by our stationary and mobile monitoring very low frequency (VLF) radio stations. These signals were classified and divided into groups according to their source. Capturing of natural origin signals and their spectral patterns together with the time of their origin seem to confirm our assumption about the correlation between deformations in the slope and electromagnetic (EM) anomalies in the radio spectrum after further analysis. We conclude that since we always observe them a few days to hours after heavy rainfall and they are not observed at both stations at the same time, it confirms that they represent local phenomena not caused by atmospheric or ionospheric processes or events but deformation in landslide body microfracturation and microdisplacements via piezo-electromagnetic effect. Also, at the time after capture, it is possible to observe changes in the terrain in the form of new cracks of a sub-meter size. The EM field around the VLF band, DC – 30 kHz (up to 24 kHz in our measurement) was recorded using sound cards that served as an AD/DA converter. The VLF monitoring station and mobile measurements were located on the landslide slopes.

**Key words:** geodynamics, natural radio emission, VLF, manmade noise, landslide

## 1. Introduction

Presented here are preliminary results of occurring spectral patterns obtained by us over 3 years by 24/7 permanent observations. The preliminary catalogue of those spectral patterns also helps to identify natural radio spectral patterns and to distinguish them from sources of electromagnetic energy of artificial (anthropogenic) origin. Recordable electromagnetic (EM) field in nature could diverse a lot. There are diverse natural EM fields generated by natural phenomena such as lightning (*Inan et al., 2010*), wind (*Bo et al.,*

2013) (triboelectric effect of particles carried by wind due to rubbing against each other and the surface), sun (solar wind effects in the upper layers of the atmosphere), earthquakes (*Hanson and Rowell, 1980; Gershenzon and Bambakidis, 2001; Hayakawa, 2015, Rabinovitch et al., 2000*) and landslides (*Maniak, 2015; Kharkhalis, 1995; Kóktavý and Šikula, 2004*). The second basic type is the artificial (anthropogenic) EM field due to human activity. Geophysicists have encountered EM noise at different frequencies at different times and latitudes during field EM measurements (*Blaha and Duras, 2004; Fabo et al., 2004*). The aim of the work is to identify, distinguish, analyse, and classify the spectral patterns of EM signals with a focus on identification of natural radio signals originating from the rock environment (see the online Supplement) particularly due to landslide related phenomena (*Kharkhalis, 1995; Vybiral, 2002*).

## 2. Geological settings

Geological structure is important when considering the rate of fracture propagation through the rock environment. This speed depends on the rock composition. In our case, we are considering crack propagation speeds of approx. 1100–2500 m/s for saturated clay and 1500–2000 m/s for wet sands (*Schumann et al., 2014*). The speed of crack propagation is calculated from the speed of seismic P wave in clays and sands. From this speed we can calculate at what frequency range we can expect radio anomalies (*Martinelli et al., 2020*). Similar research was conducted earlier (*Goldbaum et al., 2003* and *Rabinovitch et al., 2000*), but also with the application of shear stress. To calculate the expected frequency  $f_{anom}$  of radio anomalies, we used Eq. (1), where  $t_{prop}$  is the time needed for a crack to develop in the material with a length of fracture in a rock block  $l_{frac}$ , considering that the crack propagation speed could be close to the speed of seismic P waves. The length  $l_{frac}$  is a characteristic length of cracks observed in the field, formed under given conditions in the clay-sandstone rock environment:

$$t_{prop} = \frac{l_{frac}}{v_{seis}} \text{ [s]}. \quad (1)$$

We used the inverse value (Eq. (2)) of the calculated crack propagation time to calculate the cracking rate (*Martinelli et al., 2020*):

$$f_{anom} = \frac{1}{t_{prop}} \text{ [Hz]}. \quad (2)$$

In literature, different relations (Eq. (3)) can be found for calculating the frequency of the EM field generated by crack propagation, which was described by *Martinelli et al. (2020)*, as follows:

$$\omega = \frac{v_{el} \cdot \pi}{b} \text{ [s}^{-1}\text{]}. \quad (3)$$

when  $\omega$  is the EM emission frequency,  $v_{el}$  represents the Rayleigh velocity and  $b$  is the width of the fracture. However, *Martinelli et al. (2020)* use the Rayleigh velocity, while we used the velocity of seismic P waves, since we are considering material compression only. Our study area is located in the Hlohovec – Sereď landslide zone in the cadastre of the municipalities of Vinohrady nad Váhom and Dvorníky. The geological structure (Fig. 1) is represented by Pliocene and Quaternary sediments (*Harčár and Priechodská, 1988*). Pliocene sediments occur throughout the territory at depths of 0.3–7.0 m on the uplands and 8.0–20.0 m at the river Váh floodplain. The Pliocene assemblage is represented by continuous clay layers from tens of meters to several centimetres thick. This arrangement of sandstone and clay loam with alternating layers forms favourable conditions for the origination of slope deformations (*Otepka et al., 1983*).

Quaternary sediments are formed by fluvial and eolian sediments with a thickness of 0.5–15 m. The fault of river Váh is the most important tectonic line. Locally, it runs N-S and separates the Nitra upland from the river Váh bottom land (*Leško and Tichý, 1963*). The valleys are oriented diagonally to the fault of river Váh, which indicates their tectonic origin, and are trench depressions 100–500 m wide (*Adam and Dlabáč, 1961*).

### 3. Material and methods

A BEHRINGER UMC HD 204 sound card with a maximum sampling of 192 kHz was used to receive radio waves in the VLF band, with a radio band width from DC to 91.5 kHz (in our case, we monitor the radio band up to 24 kHz), (<https://www.behringer.com/product.html?modelCode=POBKO>).

There we used a 40-threaded Air coil with an amplifier based on OP27 and an earth dipole without additional amplifiers with a length of at least

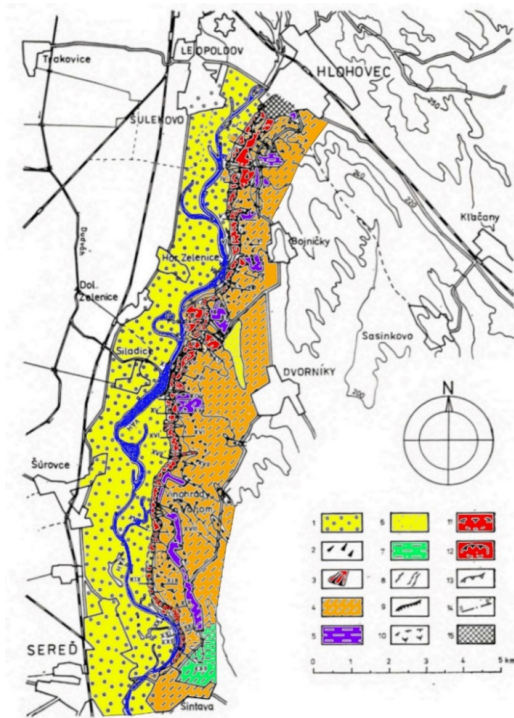


Fig. 1. Schematic geological map of slope failures in the territory between Hlohovec and Sered. 1 – fluvial deposits, 2 – piedmont soil-sandy deposits, 3 – alluvial cones, 4 – eolitic-deluvial and deluvial sediments (1 to 4 – Quaternary), 5 – clay, sandy and dusty clay, 6 – sand, clayey sand, 7 – alternation of sandy and clayey sediments (5 to 7 – Neogene), 8 – erosion runnels, 9 – side erosion of Váh river, 10 – surface crawling, 11 – slides of first and second generation, 12 – slides of third generation, 13 – soil collapse, 14 – line of engineering-geological sections, 15 – fills, made-up grounds (modified *Otepka et al., 1983*).

50 m as an antenna system for VLF reception (Figs. 2 and 3). The signal from the antenna system was processed on the sound card and sent in RAW form to the imaging and analysis software. The Spectrum Lab software (*Buescher, 2020*) was used in this case (Fig. 4). It is possible to connect both antenna systems to the sound card at the same time through the left and right channels (e.g., the air coil to the left channel and the ground dipole to the right channel). Switching the channels enables to monitor both at the same time or use them in a Radio Direction Finder (RDF)



Fig. 2. Setting of mobile VLF acquisition system on landslides body with loop and earth probes antenna system and their amplifier system like Kamenica and Stoček (second permanent VLF station) monitoring station. The antenna is on a tripod for easier routing to remove unwanted noises from the village, the earth probes antenna system is 80m long and is directly connected to the sound card as the right channel with the same 192 kHz sampling (Landslide Motocross 2022).

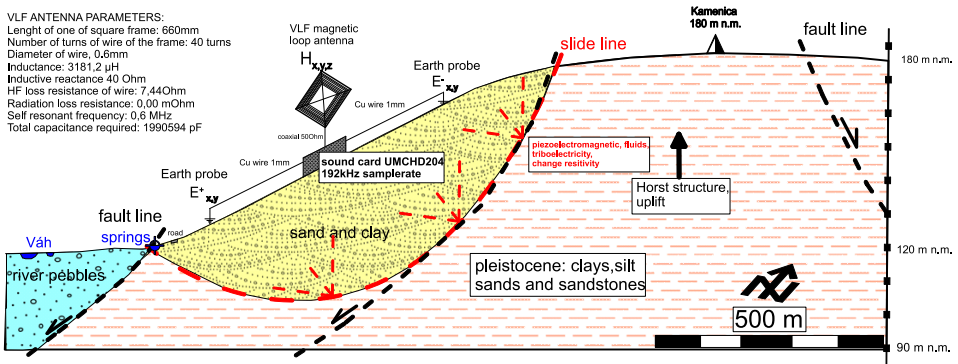


Fig. 3. Location of the VLF Air-loop antenna and the VLF ground dipole in the field – sketch.

mode. The station is located in a small weatherproof building (protected from weather conditions, mainly wind, rain and sudden changes in tempera-

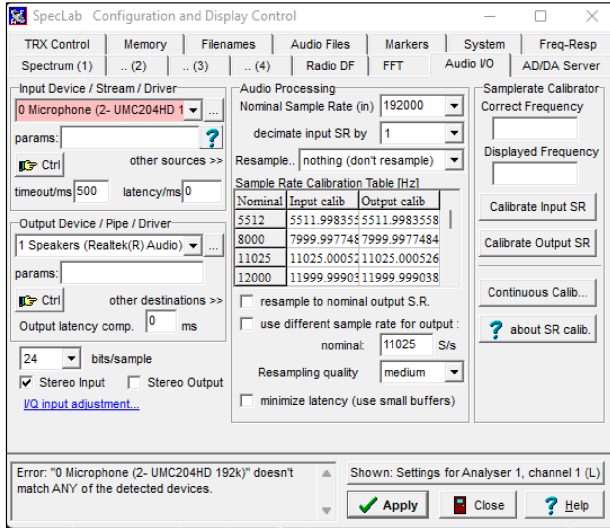


Fig. 4. Spectrum Lab input device settings: Input device (UMC204 HD external sound card), 24 bits/sample (for two dipoles system must set “stereo input”, for mono antenna system unset “stereo input”). Nominal sample rate from 5512 Hz to 192 kHz, Output: default (for send data to other analyser you can use virtual cable like software). This menu is also used for automatic calibration.

ture) with N–S (parallel to the slope line for obtaining a signal from a wider area of landslide body) orientation, located approximately at one third of the slope, 1 m below the ground. Antenna parameters: length of one square frame: 660 mm; number of turns: 40; Diameter of wire is 0.6 mm; Inductance is 3181.2  $\mu\text{H}$  with inductive resistance 40 Ohm; HF loss resistance of wire 7.44 Ohm; self-resonance frequency: 0.6 MHz and total capacitance required is 1990594 pF. Antenna is connected via short audio cable with shielding as broad-band H-Field antenna.

The exact description of the methodology of recording the EM field in the VLF band is described in due detail by *Hoffman (2022)*. The purpose of two or more VLF monitoring stations (mobile or remotely controlled permanent) dwells in the comparison of signals captured at one VLF station to the other, for the sake of excluding atmospheric and ionospheric sources of EM anomalies and confirming the local source. We can also focus the source azimuthally using the radio direction finder (RDF) function. This is here, however, outside the scope and will be subject of future work.

Division into the two categories – natural and artificial signals – is performed based on the fact that natural signals are compared with known signals from published literature, especially (*Helliwell, 1965*) and (*Martinelli et al., 2020*). Artificial signals (their spectral patterns) are recognized based on own experience. We took the whole VLF system to an apartment, a house, a garden, and “recorded signals of various electrical devices”. Then, when we captured the same spectral patterns in the field, it was possible to assign a source to the signal recorded at the station, even if these spectral patterns, or recordings of the entire spectrum in the form of “\*.wav” audio were converted (by offset into filters) into audio frequencies, so that we could even hear the very characteristic sound of these electrical devices.

### 3.1. Calibration, quality assurance and quality control

For most geophysical apparatus and for the measurement of the EM field in the VLF band by means of a sound card, the equipment shall be calibrated and maintained in a calibrated state throughout the measurement. The uncalibrated device, while displaying the correct shape of spectral patterns, may not agree with the frequency range within which they are monitored. To calibrate the VLF receiver, we use the ‘audio I/O’ menu in the Spectrum Lab (Fig. 4) or the ‘2’ (Fig. 5) menu using the ‘radio frequency offset’ sub-menu. The difference between the two methods is that, in the first case, we use a computer oscillator (processor) for continuous calibration, which provides the correct sampling frequency.

The second method is calibration using known frequencies, e.g., military navigation transmission. In this case, we used the DHO38 transmitter from Germany at frequencies of 23.4 kHz and a transmission power of up to 300 kW, and HWU transmitter from France at frequencies of 18.3 kHz, 20.9 kHz, and 21.7 kHz and a transmission power of 200 kW. The maintenance and quality control of our permanent VLF station is carried out in the first way (continuous calibration by means of an internal oscillator), as the station is remote and operates 24/7. In campaign measurements, we used the second way to calibrate, because this approach is faster and less burdensome for the computer, saving energy. It was crucial, because of loading an EM field into the VLF band is not possible by recharging the device from the grid at the same time.

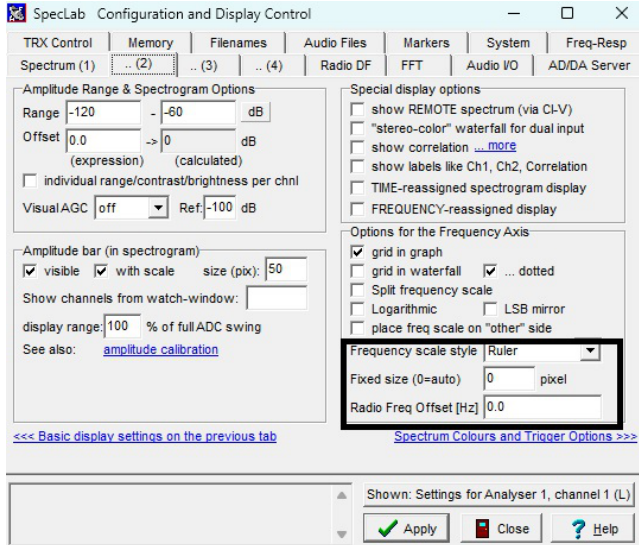


Fig. 5. Spectrum Lab menu for setting offset to known frequency. This menu also uses for setting range of spectrograph, display range for amplitude graph.

The electrical characteristic for the signal calculation follows from the Faraday-Lenz law (4):

$$V = -\frac{d\varphi(t)}{dt}, \tag{4}$$

where  $V$  is the open circuit voltage rms and  $\varphi(t)$  is the magnetic flux at time “ $t$ ”. It applies to the loop antenna:

$$V = -n \frac{d\varphi(t)}{dt},$$

where  $n$  is the number of turns, while the magnetic flux is:

$$\varphi(t) = B(t) Ae \cos(\vartheta), \tag{5}$$

where  $Ae$  is the surface of the circular equivalent loop,  $\vartheta$  is the angle between the flux lines and the orthogonal of turns plane, while  $B(t)$  is the magnetic induction field. The magnetic field of an EM wave is:

$$B(t) = B \cos(\omega t), \quad \text{with } \omega = 2\pi f, \quad (6)$$

where  $f$  is frequency. After differentiating we obtain the following relationship:

$$V = 2\pi n A e f B \cos(\vartheta). \quad (7)$$

Consequently,  $\vartheta = 0$ , because the antenna is aligned with the magnetic field propagation. Frequency  $f$  is set to 15 kHz (chosen as central frequency for receiving),  $n$  (the number of copper wire turns) is 40,  $Ae$  is equal to  $0.16 \text{ m}^2$  (calculated from geometric data and corrected according to the above formulae). Then we obtain  $V = 602.880 * B$ . We can also calculate the equivalent height of the antenna from the relationship of (*Balanis, 2016*):

$$V = h e \cdot E, \quad (8)$$

where  $he$  is equivalent height and  $E$  is electric field, equal to  $c * B$ . We then obtain:

$$h e = \frac{2\pi n A e f \cos(\vartheta)}{c}. \quad (9)$$

Consequently, we can simplify the relationship to

$$h e = \frac{2\pi n A e f \cos(\vartheta)}{\lambda}, \quad (10)$$

with  $he$  equal to 0.007 m. The electric field value of an EM wave could be  $E = 1 \text{ mV/m}$  when  $V = 7 \text{ } \mu\text{V}$  (when using OP27 based VLF amplifier). We can calculate and display the radiation pattern (Fig. 6), (*Balanis, 2016; Reeve, 2010; UKRAA*).

#### 4. Basic types of natural VLF radio emissions

*Spherical*: spherical or static EM emissions are produced by lightning. The spherical pulse has a frequency range of the order of tens of Hz up to 1 MHz. The maximum is in the band of 10 to 15 kHz. Spectrally, they are characterized by vertical spectral lines with the density of these lines depending on the number of flashes per second (*Helliwell, 1965*).

*Tweeks*: they arise similarly to spherical pulses, but they propagate to a greater distance than the earth-ionosphere waveguide. The distance

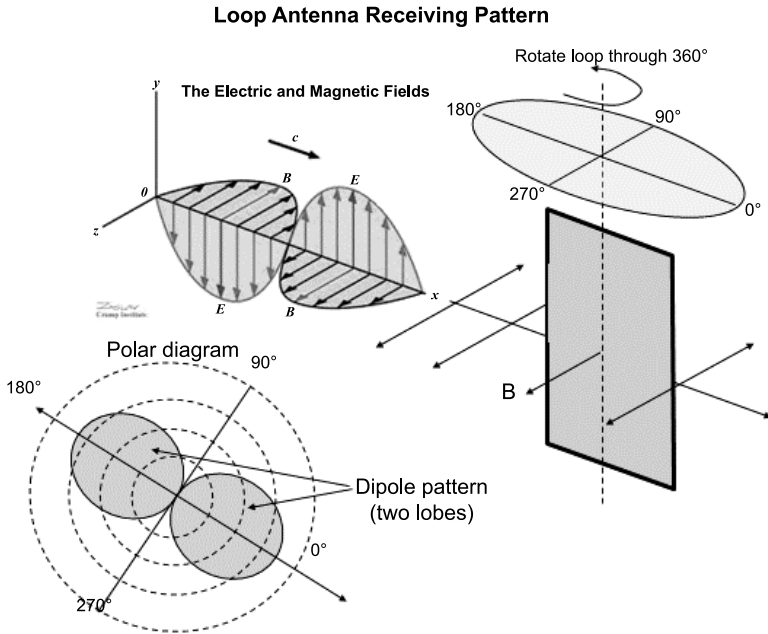


Fig. 6. Radiation pattern of VLF multiturn antenna, according to <https://www.ukraa.com/>.

could reach up to half the earth circumference. The VLF radio signal at this distance undergoes a dispersion process, where the signal at higher frequencies spreads faster than the signal at lower frequencies. The spectral image is in the form of a vertical line with a curvature (hook) around 1–3 kHz.

*Whistlers:* they arise only under the right conditions, when the VLF signal is sent from the earth to outer space and returns along the geomagnetic field lines to the conjugate point, (Parker, 1961; Dungey, 1963; Helliwell, 1965). Sequential “arrival” of frequencies could be confirmed by the appearance of the arcs on the spectrogram (Fig. 7). When converted to audio, a whistler is characterized by a whistling sound with a falling pitch, as low frequencies travel at a slower rate. Whistlers can be divided into: Pure Note Whistler, Diffuse Whistlers, Two-Hop Whistlers, and Whistler Echo Train (Helliwell, 1965). Whistlers were not captured in our observation. They are not very intense in our geographical position, and do not arise during geodynamic processes.

*Chorus*: it is probably caused by many successive whistlers in short time intervals.

*Triggered Emissions*: are EM emissions, the origin of which is caused by a previous radio emission, for example a spherical pulse. Model of spectral patterns in VLF band is described on Fig. 8.

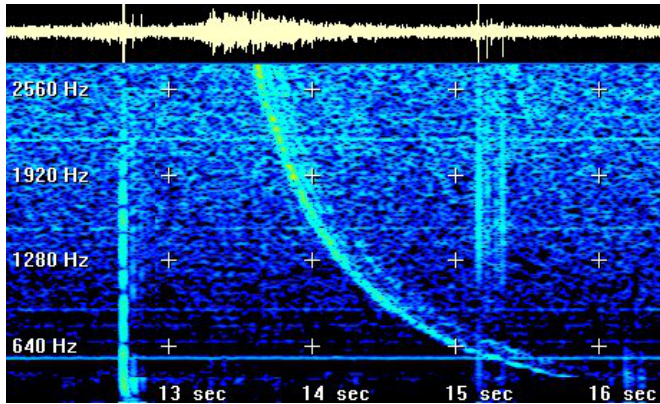


Fig. 7. Whistler with initial spherical impulse (<https://www.spaceweather.com/glossary/inspire.html>).

## 5. Results

### 5.1. Spectral patterns of anthropogenic emissions from the vicinity of the “Kamenica” landslide

The spectral patterns of the EM emission signals that we were able to capture at the Kamenica landslide site to date, related to human activities, are presented in the online Supplement, see figures A1 through A15. The sources of these EM emissions we identified as diverse, such as various electric engines or motors, of devices like grinders, circular saws, lawn mowers, pumps, sanders, carburizers, and compressors.

### 5.2. Spectral patterns from around the “Kamenica” landslide, which we attribute to natural sources

The spectral patterns of the EM emission signals that we were able to observe at the Kamenica landslide site to date, which we classify as natural, are presented in the online Supplement, see figures B1 through B12.

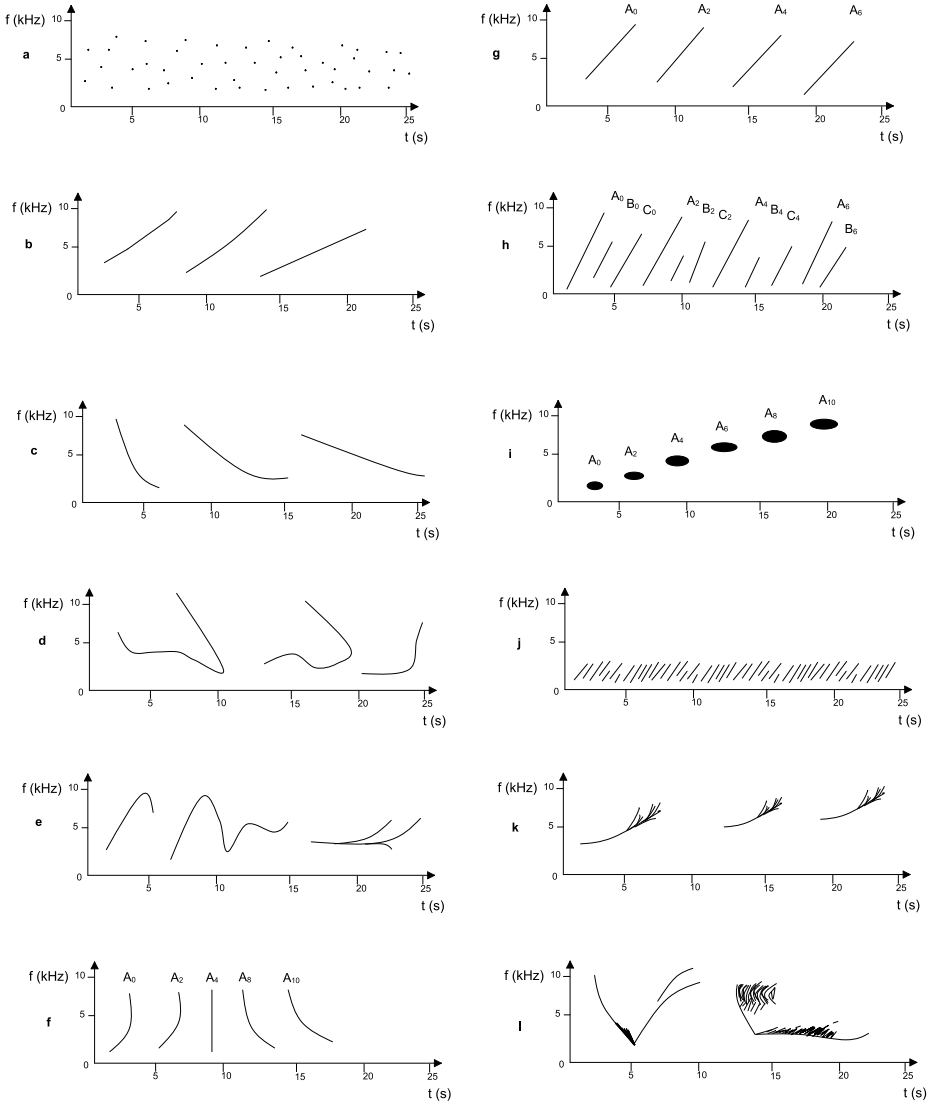


Fig. 8. Model spectral forms of VLF emissions: a) hiss, b) discrete emission-rising tone, c) discrete emission – falling tone, d) discrete emission – hook, e) discrete emission – combinations, f) periodic emission – dispersive, g) periodic emission – non-dispersive, h) periodic emission – multiphase, i) periodic emission – drifting, j) chorus, k) quasi-periodic emission, l) triggered emission (according to *Helliwell, 1965*).

These captured patterns are diverse. We relate them either to the landslide body deformation or movements, or to atmospheric/ionospheric events such as lightnings. At this site we could observe to date non-periodic (discrete and spherical) emissions, a quasi-periodic emission, chorus, combined (hook, falling and rising tone) emissions, periodic emissions (falling tone), non-dispersive emissions, and combined (hook, falling and rising tone) “triggered” emissions.

## 6. Discussion and conclusion

We recorded anomalous EM emissions and their spectral shapes by using a VLF receiver at a landslide area. The spectral patterns were divided into two categories: Spectral patterns of anthropogenic VLF radio emissions and spectral patterns which we attribute to natural sources. Each observed spectral pattern underwent identification procedure and was assigned to a source. The first group included sources such as various electrical devices, for instance mowers, grinders and other electrical appliances used in ordinary households, home workshops and garden keeping. This knowledge has helped to separate this artificially created EM noise from natural EM noise. By simple experiments with loop antenna and various types of piezo lighters (source of piezo-electromagnetic signal), we found that after compressing the piezo crystal, radio emissions were emitted in the vicinity of 4 kHz with a range of 2 kHz (this will be the subject of a separate publication). However, in the field, we often encounter artificial noise right in this zone, which has caused a problem in accurately identifying the radio emissions coming from the body of the slide. We attribute the spectral shapes in figures B1, B2, B5 and B6 (online Supplement) to geodynamic activity in the landslide body, because we always observe them for several days to hours after heavy rains and they are not observed concurrently at both VLF monitoring stations, which justifies the signal as pertaining to a local phenomenon not caused by atmospheric or ionospheric processes. In addition, at the time after capture, it is possible to observe changes in the terrain in the form of newly formed cracks with size up to a meter. This is not the case with anthropogenic.

We assigned the EM emissions presented in figures B1, B2, B5 and B6 (of the Supplement) to geodynamic activity in the sliding slope. This assumption is validated by results dealing with EM emissions arising from the

compression of quartz crystals, where very similar radio spectral shapes were observed (*Martinelli et al., 2020*). Our own experiments with piezo crystals (in lighters) also contribute to this finding, where during their compression the same anomalous spectral shapes (continuous, non-periodical, frequency around 4 kHz with 2 kHz width as in figure B2 of the Supplement) were generated, while the same equipment as that in field measurements was used to record them. The other interesting spectral shapes observed were full spectrum (see figure B5 of the Supplement) with peaks around 4 kHz, same as in the case of piezoelectric phenomena. The last interesting spectral pattern is shown in figure B6 of the Supplement, which is a combination of non-periodic radio emissions with frequency drifting from DC to approximately 10 kHz and full-spectrum spherical impulses. *Martinelli et al. (2020)* also recorded this type of spectral shapes in their laboratory experiments.

The frequency range of anomalous radio emissions was described. The analysis and understanding of piezoelectric phenomena and triboelectricity on landslides require additional time-consuming field measurements and laboratory experiments.

In the future, we are preparing an experiment with several antennas (minimum two antennas) using the DRF (radio direction finder) function using both main inputs of the sound card. We would like to use the directional feature of the H-Field antenna to monitor certain local parts of the sliding body (near field reception).

**Acknowledgements.** This work was supported by the Vega grant agency, project No. 2/0002/23.

## References

- Adam Z., Dlabáč M., 1961: Nové poznatky o tektonice československé části Malé dunajské nížiny (New insights into the tectonics of the Czechoslovak part of the Small Danube basin). *Věstník ÚÚG*, **36**, 3 (in Czech).
- Balanis C. A., 2016: *Antenna theory: analysis and design*, 4th Ed. John Wiley & Sons, p. 86: Equation (3.17).
- Bo T., Zhang H., Zhu W., Zheng X., 2013: Theoretical prediction of electric fields in wind-blown sand. *J. Geophys. Res. Atmos.*, **118**, 10, 4494–4502, doi: 10.1002/jgrd.50155.
- Buescher W., 2020: *Spectrum Lab V. 2.96 Manual*. [https://www.qs1.net/dl4yhf/specLab/SpecLab\\_Manual.pdf](https://www.qs1.net/dl4yhf/specLab/SpecLab_Manual.pdf).

- Blaha P., Duras R., 2004: Natural high frequency electromagnetic field on the Karolinka landslide. *EGRSE, Int. J. Explor. Geophys. Remote Sens. Environ.*, **XI**, 1-2, 30–32.
- Dungey J. W., 1963: Loss of Van Allen electrons due to whistlers. *Planet. Space Sci.*, **11**, 6, 591–595, doi: 10.1016/0032-0633(63)90166-1.
- Fabo P., Gajdoš V., Blaha P., 2004: The sources of 14 kHz EM fields observed at geo-electrical measurements. *EGRSE, Int. J. Explor. Geophys. Remote Sens. Environ.*, **XI**, 1-2, 23–26.
- Gershenson N., Bambakidis G., 2001: Modeling of seismo-electromagnetic phenomena. *Russ. J. Earth Sci.*, **3**, 4, 247–275, doi: 10.2205/2001es000058.
- Goldbaum J., Frid V., Bahat D., Rabinovitch A., 2003: An analysis of complex electromagnetic radiation signals induced by fracture. *Meas. Sci. Technol.*, **14**, 10, 1839–1844, doi: 10.1088/0957-0233/14/10/314.
- Hanson D. R., Rowell G. A., 1980: Electromagnetic radiation from rock failure. Report of Investigation no. 8594, Colorado School of Mines, Colorado, USA.
- Harčár J., Priechodská Z., 1988: Vysvetlivky ku geologickej mape severovýchodnej časti Podunajskej nížiny (Explanatory notes to the geological map of the north-eastern part of the Danube Lowland). Geologický ústav D. Štúra. Bratislava. 114 p. (in Slovak).
- Hayakawa M., 2015: Earthquake prediction with radio techniques. John Wiley & Sons, Singapore Pte. Ltd., ISBN: 9781118770160, p. 125.
- Helliwell R. A., 1965: Whistlers and Related Ionospheric Phenomena. Dover Publications, Inc., ISBN 978-0-486-44572-4, originally published by Stanford University Press, Stanford, California (1965).
- Hoffman M., 2022: On potential use of natural electromagnetic emissions in ELF, VLF and HF radio bands at active landslide areas: Preliminary results from Vinohrady nad Váhom site (Slovakia). *Contrib. Geophys. Geod.*, **52**, 1, 113–125, doi: 10.31577/congeo.2022.52.1.5.
- Inan U. S., Cummer S. A., Marshall R. A., 2010: A survey of ELF and VLF research on lightning-ionosphere interactions and causative discharges. *J. Geophys. Res. Space Phys.*, **115**, A6, A00E36, doi: 10.1029/2009JA014775.
- Kharkhalis N. R., 1995: Manifestation of natural electromagnetic pulse emission on landslide slopes. *Geophys. J.*, **14**, 4, 437–443.
- Koktavý P., Šikula J., 2004: Physical model of electromagnetic emission in solids. In: Proc. 26th Eur. Conf. Acous. Emission Testing EWGAE 2004, Berlin, Germany, Deutsche Gesellschaft für Zerstörungsfreie Prüfung E.V., 1111–1117, ISBN: 3-931381-58-7.
- Leško B., Tichý Š., 1963: Inžinierskogeologický prieskum ľavobrežia Váhu medzi Hlohovcom a Sereďou (Engineering-geological survey of the left bank of the Váh River between Hlohovec and Sereď). Geologický prieskum, Bratislava, report, 56 p. (in Slovak).
- Maniak K., 2015: Measuring Electromagnetic Emissions from Active Landslides. *J. Telecommun. Inf. Technol.*, **2015**, 2, 44–51.

- Martinelli G., Plescia P., Tempesta E., 2020: Electromagnetic Emissions from Quartz Subjected to Shear Stress: Spectral Signatures and Geophysical Implications. *Geosciences*, **10**, 4, 140, doi: 10.3390/geosciences10040140.
- Otepka J., Menzelová O., Bohyník J., Mesko M., Čubříková E., Roháčiková A, Škriepková L., Novotný P., Čellár S., Abelovič J., Čerňanský J., Kúdeľa P., Bláha P., 1983: Hlohovec – Sereď, prieskum a sanácia zosuvov, orientačný inžinierskogeologický prieskum (Hlohovec – Sereď, survey and landslide reparation, indicative engineering-geological survey). IGHP Bratislava, SGÚ Bratislava, report no. 57522, 120 p. (in Slovak).
- Parker E. N., 1961: Transresonant electron acceleration. *J. Geophys. Res.*, **66**, 9, 2673–2676, doi: 10.1029/JZ066i009p02673.
- Rabinovitch A., Frid V., Bahat D., Goldbaum J., 2000: Decay mechanism of fracture induced electromagnetic pulses. *J. Appl. Phys.*, **93**, 9, 5085–5090, doi: 10.1063/1.1562752.
- Reeve W. D., 2010: Application of the UKRAA Very Low Frequency Receiver System. [https://www.reeve.com/Documents/LF-VLF/Reeve\\_SARA%20WestConf%20VLF%20Paper\\_Upd.pdf](https://www.reeve.com/Documents/LF-VLF/Reeve_SARA%20WestConf%20VLF%20Paper_Upd.pdf).
- Schumann K., Stipp M., Behrmann J. H., Klaeschen D., Schulte-Kortnack D., 2014: *P* and *S* wave velocity measurements of water-rich sediments from the Nankai Trough, Japan. *J. Geophys. Res. Solid Earth*, **119**, 2, 787–805, doi: 10.1002/2013JB010290.
- UKRAA site: UK Radio Astronomy Association. <https://www.ukraa.com/>.
- Vybiral V., 2002: The PEE method helps assess slope stability. Laboratory and Field Observations in Seismology and Engineering Geophysics, Institute of Geonics of the AS CR, Ostrava – Poruba, Czech Republic.